fluenced by the Shuttle. The field will no longer be spherically symmetric. Angular momentum will not be conserved and the calculation becomes invalid. The theory predicts that if the probe is well behind the Shuttle, its equilibrium potential will become increasingly negative as its radius is reduced approaching minus infinity as the radius squared approaches zero. The following argument will be used to show that the potential in fact will approach some finite limiting value and not minus infinity. For an ion to reach the center of an r^{-2} field it must have zero angular velocity. As shown in the figure, this requires a substantial thermal velocity perpendicular to the drift velocity.

The approximate thermal radial velocity of zero angular momentum ion is

$$v_r = \left(\frac{p}{1}\right) v \tag{9}$$

The current density seen by a very small object in the center of the wake is approximately

$$i = i_0 \left(1 + \frac{2qV}{mv^2}\right) \exp\left[-\left(\frac{pv}{1}\right)^2 \frac{m}{2kT_i}\right] \tag{10}$$

where i_0 = undisturbed ion drift current density. The approximate current balance equation is then

$$i = i_0 \left(1 + \frac{2qV}{mv^2}\right) \exp\left[-\left(\frac{pv}{1}\right)^2 \frac{m}{2kT_i}\right] = i_0 \exp\left(\frac{qV}{kT_e}\right) \tag{11}$$

This then gives the limiting potential as r_p approaches zero. Note that this equation determines how far behind the Shuttle wake effects dominate charging. The effective wake length is roughly:

$$1 = pv\left(\frac{m}{2kT}\right)^{1/2} \tag{12}$$

Conclusions

The Manned Maneuvering Unit can charge to about -1400 volts in the wake of the Shuttle as an oxygen ion plasma. One percent hydrogen would lower the potentials by 14%, and 6% hydrogen would reduce the potential by a factor of two. The presence of a higher percentage of hydrogen ions at higher altitudes would substantially decrease the maximum potential. Is a potential of -1400 volts hazardous to the man in the Manned Maneuvering Unit? Perhaps a spark will occur when the unit touches the Shuttle. This potential, if sufficiently nonuniform on the MMU surface, may produce a surface discharge. Radiation from these arcs may be harmful to electronics in the vicinity and therefore affect the MMU mission.

References

[1]Konradi, A., NASA Johnson Space Center, 1983, private communication.

[2]Shuman, B.M., Vancour, R.P., Smiddy, M., Saflekos, N.A. and Rich, F.J., "Field-Aligned Current, Convective Electric Field, and Auroral Particle Measurements During a Major Manetic Storm," *Journal of Geophysical Research*, Vol. 86, 1981.

Radiative and Convective Effects on the Vibrational Heating of Semitransparent Polymers

I.S. Habib*
University of Michigan—Dearborn
Dearborn, Michigan

Nomenclature

A_r = a constant related to the effect of temperature on viscosity
a_r = Rosseland absorption coefficient for the optically thick limit
Bi = Biot number, $= hL_c/k$
k = thermal conductivity of medium
L = slab half thickness, L_c = characteristic length, with L for planar geometry and R for cyclindrical and spherical geometries
N = radiation-conduction parameter for the optically thick limit defined as $N = 16\, n^2 \sigma T_\infty^3 / 3a_r k$
n = material index of refraction
q_r = radiative heat flux; q_{r1} = radiative heat flux at the surface
R = radius of cylindrical and spherical samples
T = temperature; T_s = surface temperature; T_0 = centerline temperature at $x = L$ or $r = 0$; T_1 = effective slip temperature at boundary; T_∞ = ambient temperature
x = distance from the wall
β = dimensionless heat generation, $= \gamma A_r L^2/k$; β_c = critical value of β
γ = $= \frac{1}{2}\tau_0^2 \omega^{1-m_B}$ with B and m being parameters
δ = $A_r T_\infty$
ξ = dimensionless distance $= x/L$ for planar geometry and $= 1 - r/R$ for cylindrical and spherical geometries
σ = Stefan-Boltzmann constant
τ_0 = stress amplitude; τ_{xy} = stress in slab; τ_{rz} = stress in cylinder
ϕ = dimensionless temperature $= A_r(T - T_\infty)$; $\phi_0 = A_r(T_0 - T_\infty)$
ψ = dimensionless temperature $= T/T_\infty$; $\psi_0 = T_0/T_\infty$; $\psi_1 = T_1/T_\infty$
ω = frequency of oscillating axial stress

Introduction

TESTING of material samples under cyclic loading may not, at times, lead to a thermal steady state in which the nonlinear rate of heat generation by the viscous resistance of the material is balanced by the rate of heat transfer from the material to its surroundings. It has been found[1,2] that testing with a constant stress amplitude leads to certain critical states beyond which thermal explosion or disintegration of the sample takes place.

In a previous study,[3] the effects of radiative transport exhibited by sample emission and absorption during cyclic loading were considered for the optically thin and thick limits. Prescribed temperatures at the boundary with an effective slip coefficient for combined conduction and optically thick radiation were imposed on the model. The results obtained from the study demonstrated the significance of the radiative transport in assessing the tolerance limit of a semitransparent sample to cyclic loading.

Received Dec. 10, 1984; revision received Feb. 28, 1985.

*Professor of Mechanical Engineering.

In an actual testing set up for cyclic loading, a sample generally induces around it air currents of magnitudes which can vary substantially from one test condition to another and from one sample geometry to another. Accordingly, Biot number becomes a significant parameter in determining the level of the critical states leading to thermal failure. It is important to mention that the present problem is very similar to that experienced in heat explosion theory recognized in exothermic chemical reactions.[4,5]

The intent of this note is to examine the effect of Biot number on the critical states leading to the thermal failure of a sample under cyclic loading. Such an effect is examined in the presence of nonlinear heat generation and optically thick radiation with an effective slip for combined conduction and radiation. Although planar and cylindrical samples are generally used for cyclic testing, the spherical geometry is included in the analysis since the results thus obtained can be easily used to obtain critical limits in exothermic chemical reaction problems.

Analysis

In the optically thick limit and with a nonlinear heat generation term due to cyclic loading within the sample, the energy equations can be expressed as[3]

$$\frac{1}{(1-\xi)^{\alpha}}\frac{\mathrm{d}}{\mathrm{d}\xi}\left[(1-\xi)^{\alpha}(N\psi^3+1)\frac{\mathrm{d}\psi}{\mathrm{d}\xi}\right]+\frac{\beta}{\delta}e^{\delta(\psi-1)}=0 \tag{1}$$

where all terms are defined in the nomenclature. $\alpha=0$, 1, or 2 for the cases of the planar, cylindrical, and spherical geometries, respectively. The two boundary conditions invoked are the symmetry at the center of the sample, i.e.

$$\frac{\mathrm{d}\psi}{\mathrm{d}\xi}=0 \text{ at } \xi=1 \tag{2}$$

and the convection condition at the surface matched to an effective slip temperature for combined conduction and optically thick radiation with a slip coefficient given by[6]

$$\eta_1=\frac{\sigma T_{\infty}^4 n^2[\psi_s^4-\psi_1^4]}{q_{r1}} \text{ at } \xi=0 \tag{3}$$

where q_{r1} is the radiative heat flux at the surface and is given by

$$q_{r1}=\frac{-NkT_{\infty}\psi_s^3}{L_c}\frac{\mathrm{d}\zeta}{\mathrm{d}\xi}\Big)_{\xi=0} \tag{4}$$

Equation (1) when integrated from $\xi=0$ to 1 yields

$$\frac{\mathrm{d}\psi}{\mathrm{d}\xi}\Big)_{\xi=0}=\frac{1}{(N\psi_s^3+1)}\frac{\beta}{\delta}\int_0^1(1-\xi)^{\alpha}e^{\delta(\psi-1)}\mathrm{d}\xi \tag{5}$$

Using Eqs. (4) and (5) in Eq. (3), and solving for the effective slip temperature at the wall ψ_1 we obtain

$$\psi_1=\psi_s\left[1+\frac{16\eta_1}{3a_rL_c}\frac{\beta}{\delta}\frac{1}{\psi_s(N\psi_s^3+1)}\int_0^1(1-\xi)^{\alpha}e^{\delta(\psi-1)}\mathrm{d}\xi\right]^{1/4} \tag{6}$$

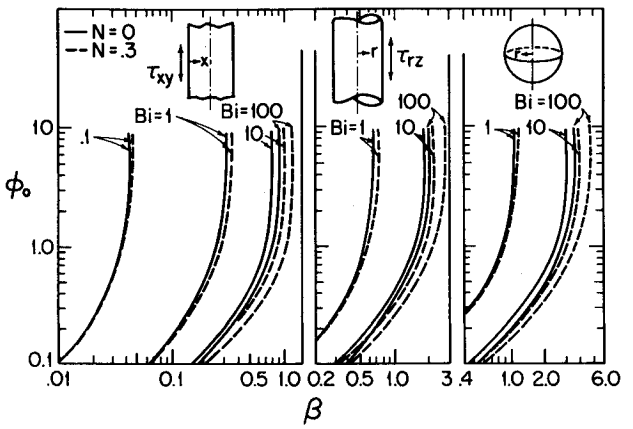

Fig. 1 Centerline temperature of the samples, $a_rL_c=5$; $Bi=hL_c/k$.

Table 1 The critical values for β_c as a function of Biot number and N; ($a_rL_c=5$; $T_{\infty}=291$ K)

	β_c					
	Planar		Cylindrical		Spherical	
Bi	$N=0$	$N=0.3$	$N=0$	$N=0.3$	$N=0$	$N=0.3$
∞	0.88	1.25	2.0	2.70	3.32	4.5
100	0.85	1.15	1.90	2.60	3.30	4.35
10	0.76	0.95	1.74	2.15	3.0	3.50
1	0.31	0.33	0.69	0.70	1.10	1.20
0.1	0.046	0.047	0.075	0.08	0.16	0.22

Equation (6) shows that as the optical depth (a_rL_c) becomes very large, the surface temperature ψ_s and the slip temperature ψ_1 becomes equal. ψ_s is determined from an energy balance at the boundary accomodating convection, conduction, and radiation, i.e.

$$(N\psi_s^3+1)\frac{\mathrm{d}\psi}{\mathrm{d}\xi}\Big)_{\xi=0}=\frac{hL_c}{k}(\psi_s-1) \tag{7}$$

Using Eq. (5) in Eq. (7) and solving for the surface temperature there results

$$\psi_s=1+\frac{\beta}{\delta Bi}\int_0^1(1-\xi)^{\alpha}e^{\delta(\psi-1)}\mathrm{d}\xi \tag{8}$$

Integrating Eq. (1) twice yields the following nonlinear integral equation.

$$\psi=\psi_1-\frac{N}{4}(\psi^4-\psi_1^4)+\frac{\beta}{\delta}\int_{\xi}^1 K_1(\xi,t)e^{\delta[\psi(t)-1]}\mathrm{d}t$$
$$+\frac{\beta}{\delta}\int_0^{\xi}K_2(\xi,t)e^{\delta[\psi(t)-1]}\mathrm{d}t \tag{9}$$

where $K_1(\xi,t)$ and $K_2(\xi,t)$ are given by:

planar: $K_1(\xi,t)=\xi$; $K_2(\xi,t)=t$

cylindrical: $K_1(\xi,t)=-(1-t)\ln(1-\xi)$

$K_2(\xi,t)=-(1-t)\ln(1-t)$

spherical: $K_1(\xi,t)=\dfrac{\xi(1-t^2)}{1-\xi}$;

$K_2(\xi,t)=t(1-t)$

Results and Conclusions

Equation (9) is solved by the method of successive approximations in which the slip and wall temperatures ψ_1 and ψ_s are evaluated from Eqs. (6) and (8), respectively, for each iteration. Initially, a temperature profile for $\psi(\xi)$ is assumed and used in Eq. (8) to evaluate ψ_s for a set of the parameters *Bi*, β, δ, N, and the optical depth $a_r L_c$. Subsequently, ψ_1 is obtained from Eq. (6) and used in Eq. (9) to generate a new set of values for ψ_s at every increment in ξ. Values for the slip coefficient η_1 are obtained from Ref. 6 as a function of the radiation-conduction number N. The newly obtained values for $\psi(\xi)$ are reused in Eqs. (8), (6) and (9), and the procedure is repeated until a convergence to the correct value of $\psi(\xi)$ is reached. The number of iterations for each run varied from four to seven in order to meet a tolerance of 0.5%. The results for a nonradiating medium with a prescribed wall temperature are independent of A_r when plotted as ϕ vs β and ϕ vs ξ,[2,3] where $\phi = \delta(\psi - 1) = A_r(T - T_\infty)$.

For a radiating medium, A_r and δ (or T_∞) must be specified. A representative value for $A_r = 0.02$ $\bar{K}^{-1}$ at $T_\infty = 291$ K was chosen and kept constant in the analysis. The present results are also shown in terms of ϕ in order to be consistent with the analysis of the nonradiating medium.

Table 1 shows the critical values for β_c as a function of Biot number *Bi* and the radiation-conduction number N. It can be seen that as the value of Biot number decreases, the critical value for the heat generation parameter β_c decreases. This signifies a reduction in the sample's ability to dissipate to the ambient the energy generated, preventing the sample from attaining a steady state. The effect is more severe at lower values of *Bi*. For $Bi = 100$, β_c is slightly less than the values obtained with a prescribed surface temperature ($Bi = \infty$). A reduction in *Bi* from 100 to 10 resulted in a reduction in β_c of 12.8% for the planar geometry. However, a reduction in *Bi* from 10 to 1 yielded a reduction in β_c of 60%. This percentage reduction in β_c is even far greater for lower values of *Bi*. The cylindrical and spherical geometries behaved in a similar way. The presence of radiative transfer in the analysis tends to increase the value of β_c and hence raises the tolerance of the sample to a higher limit of cyclic loading.

Figure 1 shows the centerline temperature of the sample as a function of β for the three geometries considered. Included also are the results for the case of a radiating medium with a radiation-conduction number equal to 0.3. The figure shows that the radiative effect is more significant at higher values of Biot number. This stems from the existence of a steeper temperature gradient within the sample for high values of *Bi* which in turn yields an increased value for the radiative diffusion heat flux.

References

[1]Meinkoh, D., "Heat Explosion Theory and Vibrational Heating of Polymers," *Intenational Journal of Heat Mass Transfer,* Vol. 24, 1981, pp. 645-648.

[2]Schapery, R.A., "Thermomechanical Behavior of Viscoelastic Media with Variable Properties Subjected to Cylic Loading," *Journal of Applied Mechanics,* Vol 32, 1965, pp. 611-619.

[3]Habib, I.S., "Radiation Effects on Vibrational Heating of Polymers," *Journal of Spacecraft and Rockets,* Vol. 21, Sept.-Oct. 1984, pp. 496-501.

[4]Gray, P. and Lee, P.R., "Thermal Explosion Theory," *Oxidation and Combustion Reviews,* Vol. 2, 1967, pp. 1-183.

[5]Steggerda, J.J., "Thermal Stability: An Extension of Frank-Kamenetski's Theory," *Journal of Chemical Physics,* Vol. 43, 1963, pp. 4446-4448.

[6]Siegel, R. and Howell, J.R., *Thermal Radiation Heat Transfer,* McGraw-Hill Book Co., Hemisphere Publishing Corp., 1981.

Parametric Investigations of Slender Cone Nose Bluntness Effects

L.E. Ericsson*
Lockheed Missiles & Space Company, Inc.
Sunnyvale, California

A RECENT extensive parameteric investigation of nose bluntness effects[1] provides both the incentive and the means to examine in more detail the accuracy of previously developed scaling laws for hypersonic nose bluntness effects.[2] At hypersonic speeds, the bow shock generated by a blunt nose embeds the aft body in an "entropy wake" with severely reduced dynamic pressure[3] (Fig. 1). Downstream of the nose the inviscid shear flow between the body and the bow shock can be described by a similarity profile,[3] as is indicated in Fig. 1. As a consequence, the effect of nose bluntness on the aerodynamic characteristics can be scaled using a universal scaling parameter.[2] The scaling parameter accounts for the combined effects of nose bluntness and aft body geometry (the frustum cone angle in the case of a slender cone). A check against available experimental results[4] indicated that the experimental data scatter may be larger than the error introduced by the approximations leading to the universal scaling concept.[2]

Figure 1 illustrates how the nose bluntness generates an inviscid shear flow, the entropy wake, in which the aft body geometry is embedded. The entropy wake increases with increasing nose drag, where the nose drag is determined by the drag coefficient C_{D_N} and the physical size of the nose. The figure illustrates how the same inviscid shear flow profile is generated by the three different nose geometries. The location of the flare surface in this shear flow can be shown[2] to be determined by (see Fig. 2)

$$\chi_\ell = C_{D_N}^{-1/2}(r_B/d_N)(r_B/\ell) \tag{1}$$

For a slender cone, the scaling parameter becomes[2]

$$\chi_{\ell_0} = C_{D_N}^{-1/2}(r_B/d_N)(r_B/\ell_0) \tag{2}$$

Where ℓ_0 is the length of the sharp cone, i.e.

$$r_B/\ell_0 = \tan\theta_c \tag{3}$$

For hemispherical nose bluntness, $C_{D_N} = 0.9$ and Eqs. (2) and (3) give

$$\chi_{\ell_0}^{-1} = 1.9\,\frac{d_N/d_B}{\tan\theta_c} \tag{4}$$

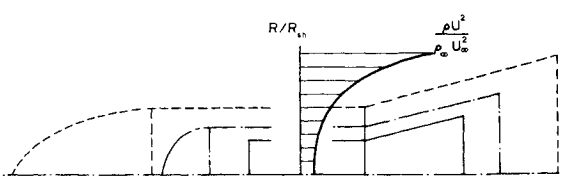

Fig. 1 Effect of nose bluntness on aft body location in "entropy wake."

Received April 6, 1984; revision received March 22, 1985.

*Senior Consulting Engineer. Fellow AIAA.